Journal of Renewable and Sustainable Energy

Analysis of the cloud enhancement phenomenon and its effects on photovoltaic generators based on cloud speed sensor measurements

Cite as: J. Renewable Sustainable Energy **12**, 043502 (2020); https://doi.org/10.1063/5.0007550
Submitted: 15 March 2020 . Accepted: 15 June 2020 . Published Online: 14 July 2020

Kari Lappalainen, and Jan Kleissl

Journal of Renewable and Sustainable Energy ARTICLE scitation.org/journal/rse

Analysis of the cloud enhancement phenomenon and its effects on photovoltaic generators based on cloud speed sensor measurements

Cite as: J. Renewable Sustainable Energy **12**, 043502 (2020); doi: 10.1063/5.0007550
Submitted: 15 March 2020 · Accepted: 15 June 2020 ·
Published Online: 14 July 2020

View Online Export Citation CrossMark

Kari Lappalainen[1,a] and Jan Kleissl[2,b]

AFFILIATIONS

[1]Tampere University, Electrical Engineering Unit, P.O. Box 692, FI-33101 Tampere, Finland
[2]Department of Mechanical and Aerospace Engineering, University of California, San Diego, California 92093-0411, USA

[a]Author to whom correspondence should be addressed: kari.lappalainen@tuni.fi
[b]jkleissl@ucsd.edu

ABSTRACT

The irradiance incident on photovoltaic (PV) generators can considerably exceed the expected clear sky irradiance. Due to this phenomenon, called cloud enhancement (CE), the maximum power of the PV generator can exceed the rated power of the inverter connecting the generator to the grid. CE event characteristics and the effects of CE on the electrical operation of PV generators were studied based on measured irradiances and cloud edge velocities. Over eleven months in San Diego, California, the highest measured peak irradiance was 1466 W/m^2. In addition, the highest simulated average irradiances for up to 1 MW generators were over 1400 W/m^2. The largest lengths for CE events exceeding 1000 W/m^2 were multiple kilometers. These results indicate that even large utility-scale PV power plants can be affected significantly by CE events. Moreover, the operation of three PV plants was simulated during around 2400 measured CE events with a detailed spatiotemporal model. The effects of inverter sizing on the operation of the plants were also studied, and the negative impacts of CE on the operation of PV systems were shown to increase with the increasing DC/AC ratio. During the CE events, the energy losses due to power curtailment were from 5% to 50% of the available energy production. While CE affects the operation of the PV plants, these effects were small in terms of aggregate energy since CE events that most strongly impact PV system operation are very rare, meaning that CE does not cause major problems for the operation of PV systems.

I. INTRODUCTION

The operation of photovoltaic (PV) generators depends on the irradiance incident on the PV cells of a generator. While solar radiation is variable (Tomson, 2013; Lappalainen and Valkealahti, 2015), the nominal electrical characteristics of PV modules are typically defined under the standard test conditions (STC), i.e., at an irradiance of 1000 W/m^2 and a cell temperature of 25 °C. However, these conditions are rare in practice. In many parts of the world, clear sky irradiance, i.e., the global irradiance from cloudless sky, can be higher than the STC irradiance around solar noon (Badescu, 1997). Moreover, on partly cloudy days, irradiance can considerably exceed the expected clear sky irradiance due to a phenomenon called cloud enhancement (CE), irradiance enhancement (Pecenak *et al.*, 2016), or overirradiance (Yordanov *et al.*, 2013a).

Irradiance levels exceeding 1000 W/m^2 (depending on module temperature) can cause the actual power of the generator to exceed its nominal maximum power. Zehner *et al.* (2011) reported up to 30% higher power output of PV modules under high irradiance conditions compared to the STC. High irradiance conditions can lead to the maximum PV power exceeding the maximum DC power of the inverter connecting the PV generator to the grid. Moreover, PV capacity is typically oversized such that the nominal DC power of the PV generator is higher than the inverter nominal (AC) power (Wang *et al.*, 2018). If the maximum power of the PV generator is higher than the maximum DC power of the inverter, the inverter will operate in power limiting mode: by moving the inverter operating point to higher voltages than those at the global maximum power point (MPP) of the generator, the current and power of the inverter decrease.

In addition to the loss of available energy production, operating in power limiting mode negatively effects the operation and efficiency of the inverter: (i) the efficiency of some inverters decreases with increasing DC side voltage (Rampinelli *et al.*, 2014), causing further

losses in AC power output. (ii) The inverter capacitor lifetime shortens with increasing DC voltage (Hasegawa *et al.*, 2018; Callegari *et al.*, 2019). (iii) Under extreme conditions, the voltage required to reduce output power may be outside the allowed voltage range of the inverter.

Under clear sky conditions, irradiances exceeding 1000 W/m^2 are typically not an issue as the exceedance is less than 10% in most areas of the world (except for high altitudes) and PV efficiency losses due to high module temperature typically far exceed 10% compared to PV efficiency at 25 °C. However, during CE, irradiance can be much larger and PV temperatures are typically lower. Gueymard (2017a) postulated that there are three types of CE effects that can strongly increase global horizontal irradiance (GHI): (1) the traditional explanation of the CE phenomenon: the enhancement of irradiance due to cloud edges near the solar disk; (2) increase in diffuse horizontal irradiance under a homogenous cloud deck before and after a CE event; and (3) partial obscuration of the sun by a thin cloud layer, while most of the sky is covered by bright clouds. In type 3, the share of diffuse irradiance is large, while the amount of direct horizontal irradiance is much lower than that in types 1 and 2. Yordanov *et al.* (2013a) demonstrated that the strongest CE is due to strong forward scattering within a small angle around the solar disk. That kind of a situation may occur when the sun appears in a narrow gap between clouds within 5° around the solar disk, which are thin enough to strongly forward scatter. The increase over 1000 W/m^2 can be substantial: Gueymard (2017b) measured a global tilted irradiance (GTI) of almost 2.0 kW/m^2 for a tilt angle of 40° and a GHI of almost 1.9 kW/m^2 in Colorado at 1829 m elevation, do Nascimento *et al.* (2019) reported a GHI of over 1.8 kW/m^2 at elevations of 392 m and 32 m in Brazil, and Yordanov *et al.* (2015) measured a GTI of 1.6 kW/m^2 near the sea level at a latitude close to 60°N.

Although CE is a well-known phenomenon, its characteristics relevant to the operation of PV systems, such as the duration and spatial extent, have not received much attention. The durations of CE events were studied in some articles: Yordanov *et al.* (2013a) presented duration distributions for CE events exceeding 1100 W/m^2; Zhang *et al.* (2018) studied the duration of CE events exceeding clear sky irradiance; and Järvelä *et al.* (2020) studied the duration of CE events with various irradiance limits over the land area of various PV generators. Järvelä *et al.* (2018, 2020) studied the land area lengths of CE events in Finland based on irradiance measurements, by invoking Taylor's hypothesis. They found typical CE event lengths to be on the order of hundreds of meters. Espinosa-Gavira *et al.* (2018) showed that CE can extend over land areas of 15 × 15 m. Weigl *et al.* (2012) showed that the land areas of CE events can be large enough to affect the operation of utility-scale PV power plants.

The effects of CE on the operation of PV systems have been studied in few articles: Zehner *et al.* (2011) studied the operation of individual PV modules under CE; Luoma *et al.* (2012) studied inverter sizing and energy losses due to inverter saturation under CE; Weigl *et al.* (2012) studied the operation of PV systems under a single CE situation; and do Nascimento *et al.* (2019) studied the effects of CE events on the performance of PV generators focusing mainly on combiner box fuses. Tapakis and Charalambides (2014) discussed the possible effects of CE on PV inverters.

This article presents a study of CE event characteristics and the effects of CE on the electrical operation of PV generators. This study is based on measurements of GHI and cloud edge velocity from San Diego, California. First, the number, duration, and land area length of CE events exceeding various irradiance limits over the land areas of various PV generators are studied. After that, the operation of three PV plants, ranging from 20 to 200 kW, is simulated during around 2400 measured CE events exceeding 1000 W/m^2. Moreover, the effects of inverter sizing on the operation of the PV plants are studied. The main novelty of this study is that, for the first time, the detailed (down to the submodule) electrical operation of PV generators is extensively studied under CE based on actual irradiance measurements.

The rest of this article is organized as follows. Sections II A–II D introduce the measurement data and the methods used to study the characteristics of CE events in terms of irradiance. The results of these studies are presented in Secs. II E–II G. The methods used to study the effects of CE on the operation of PV generators are presented in Secs. III A and III B. Section III C illustrates the effects of CE on the operation of PV generators by two static example CE situations. The statistics during all the CE events identified in measured irradiance are presented in Sec. III D. The results are further discussed in Sec. IV, and the conclusions are given in Sec. V.

II. CLOUD ENHANCEMENT EVENTS

In this section, characteristics of CE events are studied in terms of irradiance magnitudes and enhancement durations, and for point irradiance as well as for the estimated average irradiances of various PV generator land areas. This section investigates how often and how long typical land areas of different PV generator sizes experience CE.

A. Measurement data

This study is based on measurement data of a GHI sensor (LI-200, LI-COR Inc., USA) and a cloud speed sensor (CSS) installed on the rooftop of the EBU2 building at the University of California, San Diego (UCSD) (32°52′53″N, 117°13′59″W). The GHI measurements were performed with a sampling frequency of 0.5 Hz, while the response time of the sensor is 10 μs. The CSS, presented in Fig. 1, consists of an array of nine phototransistors (TEPT4400, Vishay Intertechnology Inc., USA) (Wang *et al.*, 2016). The phototransistors form a circular sector with a radius of 29.7 cm and a central angle of 105°. Eight of the phototransistors are located at the arc of the circular sector around the ninth phototransistor that is positioned at the center of the circle. The data acquisition rate of the CSS is irregular since it requires cloud edge passages to determine cloud motion vectors (CMVs). The minimum time between produced CMVs is 11 s, which is sufficient for cloud motion estimation in the scope of this study. The procedure to calculate CMVs is presented in the Appendix. The shadow movement direction is defined as the direction where clouds come from relative to north. CMVs were determined during 62 days from October 2017 to August 2018 from which GHI measurements were also available. All these days, which compose the used dataset, were partially cloudy.

B. Identification of cloud enhancement events

A CE event is often defined by comparing measured irradiance with expected clear sky irradiance (Yordanov *et al.*, 2015; Zhang *et al.*, 2018). In that way, a CE event starts when the irradiance exceeds the clear sky irradiance and ends when the irradiance decreases below the clear sky irradiance. However, from the PV system operation point of

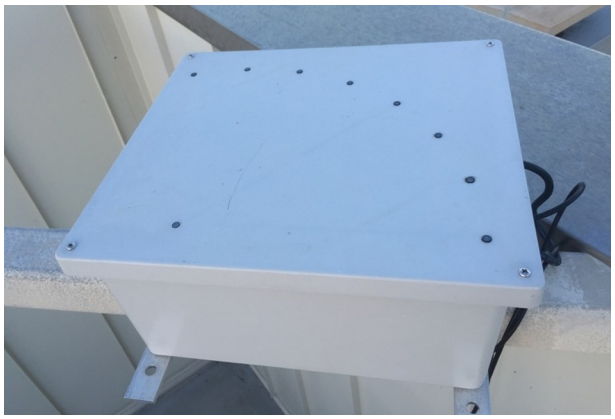

FIG. 1. Cloud speed sensor contained in an enclosure.

view, a more sensible way is to use a static irradiance value as a reference instead of the clear-sky irradiance that is location-specific. On the other hand, the use of a static irradiance value as the limit of CE events has the drawback that, depending on the location, non-CE events with large clear sky irradiance may be included, or situations with real CE during small clear sky irradiance that does not reach the static threshold may be excluded from the study. A typical static value used to define CE events is the solar constant (Zhang *et al.*, 2018). However, the use of the solar constant is not justified from the PV power operation point of view. Since the nominal ratings of PV modules are typically defined under the STC, from the PV system operation point of view, a more reasonable choice for a static threshold is the STC irradiance of 1000 W/m^2. To make the results more generalizable, instead of using a single static irradiance limit, we opted to use a continuous range of irradiance values starting from 1000 W/m^2 and identified all events where the measured irradiance, or estimated average irradiance, exceeded the irradiance limit. Then, we systematically counted the numbers and durations of these events for each irradiance limit.

C. PV generator land areas

Average irradiances over the land areas of various PV generators were estimated. The nominal powers, side lengths, and land areas of the studied virtual PV generators are compiled in Table I. The land areas are based on typical land areas of PV generators with these power ratings (Ong *et al.*, 2013). The selected power ratings correspond to typical power ratings of medium-sized (0.05 MW) and large (0.2 MW) string inverters and medium-sized (1 MW) and large (4 MW) central inverters. The PV generators were assumed to have a square shape. The shape of PV generators varies greatly in practice.

TABLE I. The powers, side lengths, and land areas of the studied PV generators.

Nominal power (MWp)	Side length (m)	Area (m^2)
0.05	25	625
0.20	50	2500
1.00	125	15 625
4.00	250	62 500

The shape of the generator affects the cumulative time the PV generators experience CE. The use of a square shape is justified as it is the most typical in practice. An oblong generator shape could distort the results more than a square shape: if one dimension of the generator is very short compared to the other, a small CE area (from a near-perpendicular direction) could fully cover the generator, while it could not cover a square-shaped generator of the same area.

D. Assumptions and estimation of 2D average irradiances

Since CE events are the result of light scattering by clouds, the speeds and movement directions of the CE areas can be estimated based on the measured CMVs. The average irradiance of the PV generator was estimated from measured point irradiance based on three assumptions: (1) Taylor's hypothesis in the streamwise direction; (2) uniformity in the cross-stream direction; and (3) the CE areas move perpendicular to the PV generator side. Through these assumptions, the CE areas can be studied one-dimensionally, allowing the straightforward calculation of the average irradiances over the PV generator land areas. The assumptions and the movement of a CE area are illustrated in Fig. 2.

The assumptions are reasonable for the studied PV generator sizes. However, Assumption 2 becomes less reasonable and the uncertainty of the results, therefore, increases with the increasing land area. Typical land area lengths of CE events have been found to be on the order of hundreds of meters up to several kilometers (Järvelä *et al.*, 2018). Typical land area diameters of cloud shadows have been reported to be around 800 m (Lappalainen and Valkealahti, 2016). The resulting CE geometries differ from those occurring in reality since cloud and scattering geometries are three-dimensional and

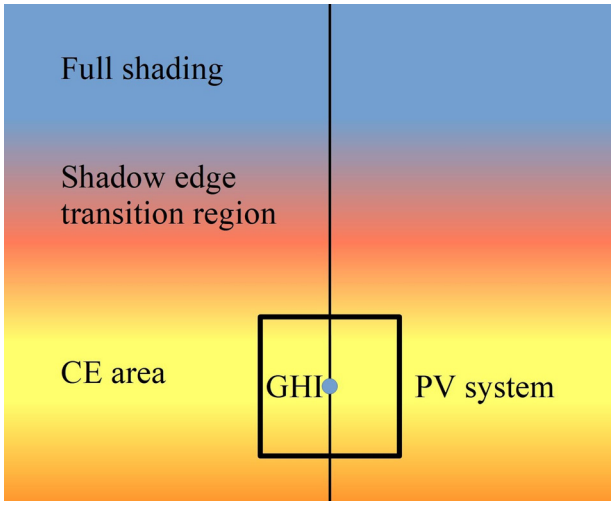

FIG. 2. Conceptual bird's eye view of a CE event that is upwind of a cloud as it impacts a PV system. Irradiance increases from blue to red to yellow. The irradiance map is generated from time series at the GHI sensor (blue dot) that is converted to a line in space aligned with the direction of cloud motion using Taylor's hypothesis (black line, Assumption 1) and extrapolated in the crosswind direction (Assumption 2). The PV system borders are assumed to be perpendicular to the direction of motion (Assumption 3).

complex. However, dense measurement networks that cover the spatiotemporal evolution of CE are not available. The extrapolation from a timeseries at a point to a line in the wind direction (1D) is well documented and reasonable based on Taylor's hypothesis, and given that the spatial scale of clouds is larger than the array sizes, the extrapolation from 1D to 2D also appears to be a reasonable assumption for the purposes of this study, which is to derive typical statistics for the effects of CE events on PV generators.

The average irradiance over the land area of the PV generator was calculated by averaging the measured irradiance over a time interval defined by the ratio of the PV generator dimension and the measured cloud shadow speed. Figure 3 presents an example of the measured irradiance and the average irradiances over PV generators of different sizes. The irradiance profile becomes smoother for larger generator land areas. The peak irradiance decreases with the increasing generator area, and all PV generators experience average irradiances exceeding 1100 W/m^2.

E. Number of cloud enhancement events

The example in Fig. 3 illustrates the effect of the generator land area on the number and duration of CE events identified in the estimated average irradiances of the generators. The irradiance measured by the GHI sensor exceeded 1000 W/m^2 eight times, i.e., the number of identified CE events for the limit of 1000 W/m^2 was eight. The estimated average irradiances of the 0.2 and 1 MW generators exceeded the limit of 1000 W/m^2 three times. For the 4 MW generator, only one CE event was identified. However, the duration of this event was about two minutes, while the smaller generators and the point measurement experienced multiple shorter CE events. The number of CE events exceeding 1200 W/m^2 was eight, four and two for the point measurement, 0.2 MW and 1 MW generators, respectively. The largest average irradiance of the 4 MW generator was 1114 W/m^2. Thus, it did not experience a CE event exceeding 1200 W/m^2.

Irradiance values larger than the STC irradiance were measured during 34 days out of 62. Figure 4 presents the daily numbers of identified CE events exceeding 1000 W/m^2. For clarity, only the days when CE was measured were included in this figure. On average, 39 CE events per day were identified in measured point irradiance. The average daily numbers of identified CE events were 24, 18, 11, and 7 for

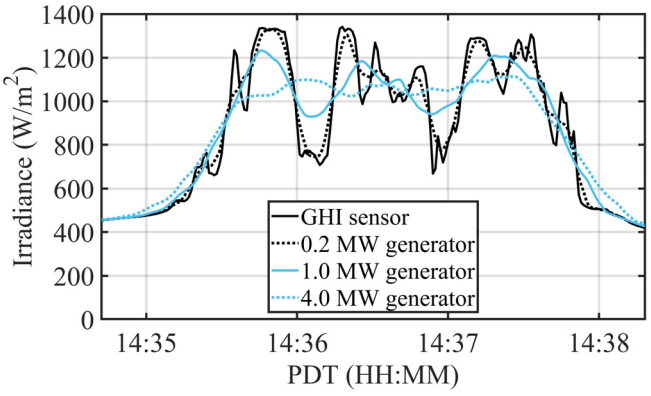

FIG. 3. Irradiance measured using the GHI sensor and the corresponding average irradiances over land areas of 0.2, 1.0, and 4 MW PV generators on May 17, 2018.

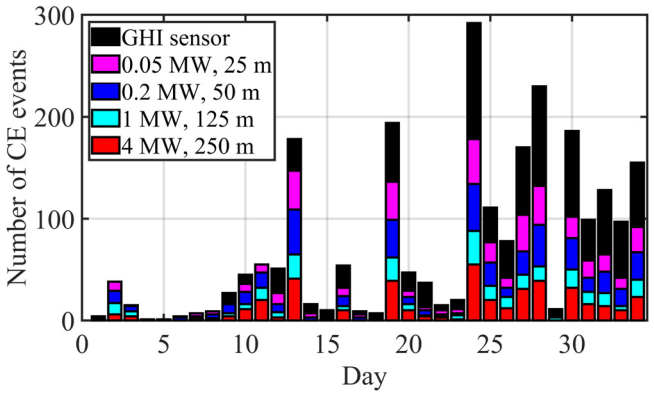

FIG. 4. Daily numbers of CE events exceeding 1000 W/m^2 for the GHI sensor and the studied PV generators. The statistics in this figure are not representative for the occurrence of CE events since only the days when CE occurred were included in the analyses.

the 0.05, 0.2, 1, and 4 MW generators, respectively. Considering only the days with measured CE events, on average, 71 CE events per day occurred in the measured irradiance. The number of identified CE events decreased with the increasing generator size due to the smoothing of irradiance with the increasing land area. The largest number of CE events was identified on May 17, 2018, with nearly 300 CE events in measured point irradiance and 55 CE events in the average irradiance of the 4 MW PV generator.

The highest irradiances measured by the GHI sensor and the highest average irradiances for the studied PV generators are compiled in Table II. The highest measured irradiance was 1466 W/m^2. The highest average irradiances for the 0.05, 0.2, and 1 MW generators were over 1400 W/m^2, i.e., over 1.4 times the STC irradiance. The highest average irradiance for the 4 MW generator was 1.34 times the STC irradiance.

The numbers of identified CE events for the studied PV generators are presented in Fig. 5 as a function of irradiance limit. The number of CE events decreased with the increasing PV generator land area and with increasing average irradiance. The measured point irradiance exceeded the STC irradiance around 2400 times during the 62 days included in the analyses. The average irradiance of the 0.05 and 4 MW generator exceeded the STC irradiance over 1500 and 400 times, respectively.

F. Duration of cloud enhancement events

The cumulative durations of identified CE events for the PV generators are presented in Fig. 6 as a function of irradiance limit.

TABLE II. Highest average irradiances for the GHI sensor and the studied PV generators over 62 days.

Area	Irradiance (W/m^2)
GHI sensor	1466
0.05 MW generator	1441
0.2 MW generator	1433
1 MW generator	1408
4 MW generator	1339

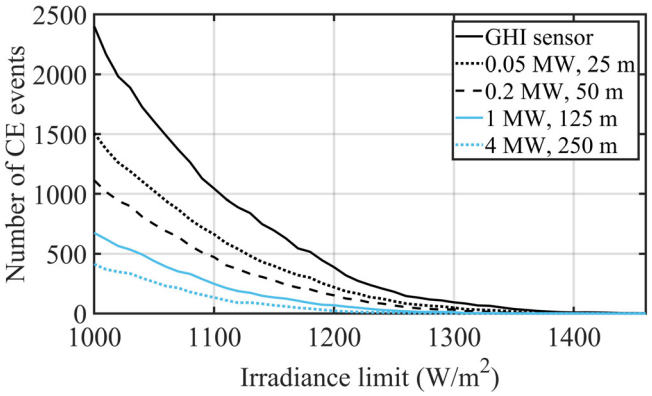

FIG. 5. Numbers of identified CE events as a function of irradiance limit.

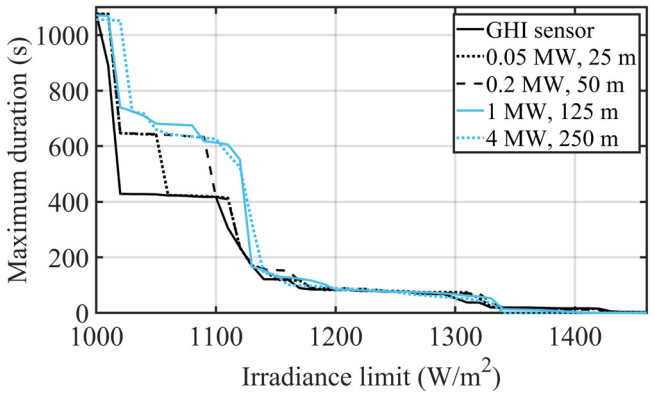

FIG. 7. Maximum durations of the identified CE events as a function of irradiance limit.

Naturally, the cumulative duration of the CE events decreased with the increasing irradiance limit and increasing land area. The cumulative durations of the CE events exceeding 1000 W/m^2 were 11 h and 27 min for the GHI sensor and 8 h and 41 min for the 4 MW PV generator. The largest cumulative duration of CE events measured by the GHI sensor in one day was 1 h and 40 min, while the average daily duration was just over 11 min, indicating that energy losses due to operation in power limiting mode during CE events are not a major issue for PV generators. The cumulative irradiance part above the STC irradiance was 12.3 kWh/m^2 for the GHI sensor and 9.2 kWh/m^2 for the 4 MW generator decreasing with the increasing land area. For reference, a typical PV generator in San Diego produces about 1500 kWh/m^2/year or 255 kWh/m^2 during the 62 days of the experiment.

Figure 7 presents the maximum durations of CE events for the PV generators as a function of irradiance limit. The maximum durations decrease with the increasing irradiance limit. The maximum durations of CE events exceeding 1000 W/m^2 were around 18 min. The average duration of these CE events was 17.2 s for the GHI sensor and increased with the increasing land area up to 75.6 s for the 4 MW PV generator. The reason for this is that small temporary dips in measured irradiance below 1000 W/m^2 are smoothed out with the larger land area, and thus, the average irradiance remains longer above 1000 W/m^2 as illustrated in Fig. 3. The longest durations of the strongest CE events with average irradiance exceeding 1400 W/m^2 were over ten seconds for the GHI sensor and the 0.05 and 0.2 MW PV generators.

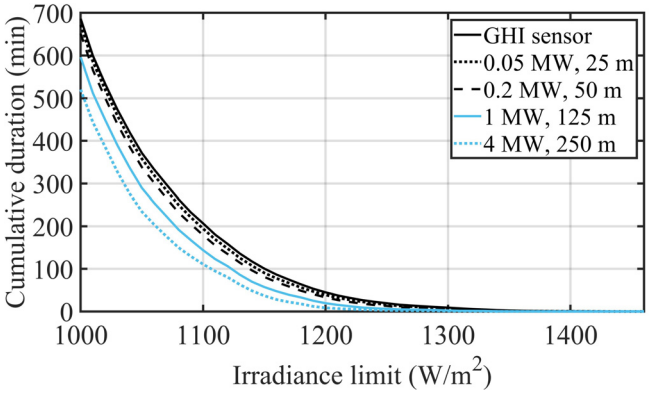

FIG. 6. Cumulative durations of the identified CE events as a function of irradiance limit.

The measured durations of CE events are broadly consistent and slightly longer than those reported in Yordanov *et al.* (2013a) and Järvelä *et al.* (2020). For example, the maximum durations of CE events exceeding 1100 W/m^2 reported in Yordanov *et al.* (2013a) and Järvelä *et al.* (2020) were around 390 and 230 s, respectively, while, in this study, a duration of 420 s was measured. The differences result mainly from the geographical location. In Yordanov *et al.* (2013a), measurements were performed in Southern Norway (latitude 58°20'N) and the sensor was oriented south (173° from North) with a tilt angle of 39° (Imenes *et al.*, 2011). In Järvelä *et al.* (2020), measurements were performed in Finland (latitude 61°75'N) with sensors oriented 23° east of due south with a tilt angle of 45°. In this study, the latitude was 32°53'N, resulting in higher clear-sky maximum irradiance values because of the smaller air mass even though GHI was measured, i.e., the sensor was not tilted. However, the measured CE event durations between these studies are broadly consistent given all the differences in the measurements.

G. Length of cloud enhancement areas

The land area length of each identified CE event was calculated by multiplying the measured duration of the event by the measured cloud shadow speed. CE area length quantiles are presented in Fig. 8 as a function of irradiance limit. The lengths of CE areas decreased with the increasing irradiance limit. The largest lengths for CE events exceeding 1000 and 1100 W/m^2 were around 6.6 and 1.2 km, respectively, meaning that even large utility-scale PV power plants can be affected by CE events. A square-shaped 16 MW PV generator with a side length of 500 m can occasionally be totally covered by a CE area with a minimum irradiance of over 1200 W/m^2. A 4 MW generator (side length 250 m) can be fully covered by a CE area with a minimum irradiance of over 1300 W/m^2. 25% and 50% of CE events exceeding 1250 and 1100 W/m^2 are large enough to fully cover a 0.05 MW PV generator, respectively. It is worth noting that the land area lengths

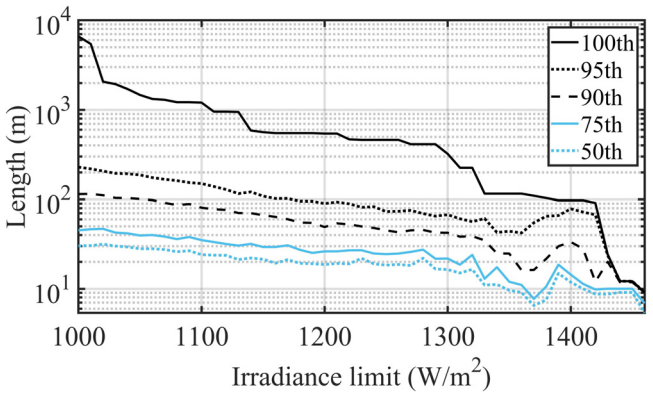

FIG. 8. 100th, 95th, 90th, 75th, and 50th percentiles of the CE area length as a function of irradiance limit.

were calculated along the CE area (cloud edge) movement direction. Naturally, full cover of PV generators requires the transverse size of a CE event also to be large enough.

III. EFFECTS OF CLOUD ENHANCEMENT ON PHOTOVOLTAIC GENERATORS

In this section, the effects of cloud enhancement on PV generators are studied by simulations. The electrical operation of three PV generators was simulated during all the identified CE events exceeding 1000 W/m^2 described in Sec. II. This section investigates how CE affects the global MPP voltage and power of the PV generators, the fraction of time the generators spend in power limiting mode, and energy losses caused by power curtailment. Moreover, the effects of inverter sizing on the operation of the PV plants were studied by varying the DC/AC ratio, i.e., the ratio of the nominal PV DC power to the nominal inverter power.

A. Simulation model for the PV modules

A PV submodule, i.e., a group of series-connected PV cells in a PV module protected by a bypass diode, was used as a basic unit in the simulations. The PV submodules were modeled by a MATLAB Simulink model, which utilizes the common one-diode model of a PV cell, providing the following relationship between current I and voltage U of a PV submodule:

$$I = I_{\mathrm{ph}} - I_{\mathrm{o}}\left(e^{\frac{U+R_{\mathrm{s}}I}{AkN_{\mathrm{s}}T/q}} - 1\right) - \frac{U + R_{\mathrm{s}}I}{R_{\mathrm{sh}}}, \tag{1}$$

where I_{ph} is the light-generated current, I_{o} the dark saturation current, A the ideality factor, T the operating temperature, R_{s} the series resistance, and R_{sh} the shunt resistance of the PV submodule. The Boltzmann constant is represented by k, N_{s} is the number of PV cells in the submodule, and q is the elementary charge. The effect of irradiance G was taken into account when calculating I_{ph} as

$$I_{\mathrm{ph}} = (I_{\mathrm{SC,\,STC}} + K_I\Delta T)\frac{G}{G_{\mathrm{STC}}}\frac{R_{\mathrm{s}} + R_{\mathrm{sh}}}{R_{\mathrm{sh}}}, \tag{2}$$

where $I_{\mathrm{SC,\,STC}}$ is the short-circuit (SC) current in STC, K_I the temperature coefficient of I_{SC}, and ΔT the temperature difference compared to STC. The bypass diodes were assumed to be at the same temperature as the submodules and were modeled using Eq. (1) by assuming I_{ph} to be zero and R_{sh} infinite. The characteristics of the simulation model were fitted to the characteristics of NAPS NP190GKg PV modules, which are composed of three submodules of 18 multicrystalline silicon PV cells. The details of the fitting process and the experimental verification of the simulation model are available in Mäki *et al.* (2012). Table III presents the SC current and open-circuit (OC) voltage of the submodule in STC and the parameter values of the simulation model.

TABLE III. Parameter values of the simulation model for the PV submodules and bypass diodes.

Parameter	Value
$I_{\mathrm{SC,\,STC}}$	8.02 A
$U_{\mathrm{OC,\,STC}}$	11.0 V
A	1.30
K_I	4.70 mA/K
N_{s}	18
R_{s}	0.110 Ω
R_{sh}	62.6 Ω
A_{bypass}	1.50
$I_{\mathrm{o,\,bypass}}$	3.20 μA
$R_{\mathrm{s,\,bypass}}$	20.0 mΩ

B. Modeling of PV generators under cloud enhancement events

The electrical operation of three PV generators was studied during the CE events exceeding 1000 W/m^2 described in Sec. II. The STC irradiance of 1000 W/m^2 was selected as the limit since the nominal ratings of PV modules and PV generators are typically defined for this irradiance. The generators consisted of 6 parallel strings of 16 series-connected PV modules, 24 strings of 20 modules, and 36 strings of 28 modules. These generator sizes correspond to typical ratings of small (6 × 16), medium-sized (24 × 20), and large (36 × 28) string inverters. The PV modules were installed facing south with a 20° tilt angle with respect to the horizon. The module strings were located in straight lines without gaps between the modules and with a 1.5 m gap between the strings. The details of the studied PV generators are compiled in Table IV.

The operation of the PV generators was studied during the movement of the identified CE events over the generators using Assumptions (1) and (2) used earlier to estimate the average

TABLE IV. Numbers of modules, powers, and dimensions of the studied PV generators.

Number of modules (parallel × series)	Nominal power (kWp)	Dimensions (m)	Area (m^2)
6 × 16	18.2	13.1 × 23.6	308
24 × 20	91.2	56.7 × 29.5	1674
36 × 28	191.5	85.9 × 41.3	3546

irradiances (see Sec. II D) with the difference that the CE areas were not assumed to move perpendicular to the PV generator side, but measured movement directions were used. Moreover, the CE area speed and movement direction were assumed to be constant, while the CE areas move over the PV generators. The speeds and movement directions for the CE events were calculated from the measured CMVs. The CMVs measured during a CE event were decomposed into north-south and east-west directions, and the median value of each was used to recompose one median filtered CMV, which was used for the CE event.

A simulation period was the period when the CE area covered at least one submodule of the PV generator, i.e., the simulation period started when the irradiance of the first PV submodule of the generator exceeded the limit of 1000 W/m^2 and ended when the edge of the CE area moved away from the last submodule. For each time step of 0.1 s, the irradiance at the center of a submodule was taken as the irradiance of the submodule. The operating temperature of the PV submodules was 25 °C during the simulations. Since temperature measurements over the land areas of the simulated generators were not available and modeling temperature under transient conditions is a challenge, we opted for this assumption. Note that Weigl *et al.* (2012) also assumed a constant PV module temperature, albeit at 40 °C. The effects of this assumption are further discussed in Sec. IV. The total duration of the identified CE events for the PV generators increased with the increasing generator land area, being around 135 h for the smallest and 208 h for the largest generator.

MPP tracking of the PV plants was assumed to be ideal, meaning that the generator is operating at the global MPP unless it is in power limiting mode, i.e., the power at global MPP is higher than the nominal power of the inverter. In that case, the generator is operating on the right-hand side of the global MPP at the lowest voltage where the nominal power of the inverter is not exceeded. The DC/AC ratio was varied from 1.0 to 2.0.

C. Static example cloud enhancement situations

The effects of CE on the operation of PV plants are first illustrated by two examples. In these examples, the CE event with the largest measured irradiance (1466 W/m^2) is located at the center of the plants. Parallel and perpendicular CE area movement with respect to the strings of the plants are considered. The irradiance levels received by the PV submodules of the plants are presented in Fig. 9, and average irradiances are compiled in Table V. The average irradiances decreased with the increasing plant size. The average irradiances of the 24×20 and 36×28 plants are larger in the case of parallel CE area movement. However, the average irradiance of the smallest plant is larger in the case of perpendicular movement.

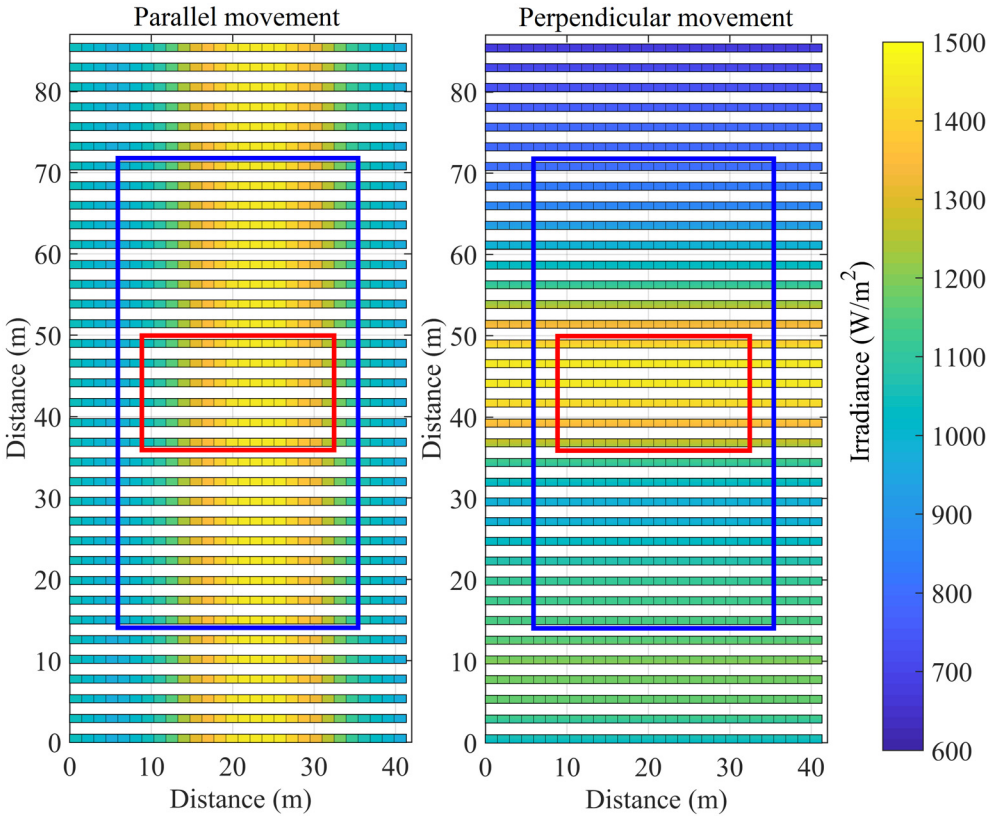

FIG. 9. Irradiance levels received by the PV submodules of the studied PV plants at 12:34 on June 5, 2018, the time of the largest measured irradiance during the experiment. The PV plants of different sizes are presented on top of each other so that the centers coincide. The modules inside the red and blue rectangle form the 6×16 and 24×20 plant, respectively. Each row of PV modules is one string.

TABLE V. Average irradiances (W/m^2) of the studied PV plants in the snapshot in Fig. 9.

PV plant	Parallel movement	Perpendicular movement
6 × 16	1335	1403
24 × 20	1286	1143
36 × 28	1211	1082

The power–voltage (*P–U*) curves of the studied generators at the same time are presented in Fig. 10. In the case of parallel CE area movement, there are irradiance differences within PV module strings. These irradiance differences cause mismatch losses (Lappalainen and Valkealahti, 2017) and lead to multiple peaks in the *P–U* curves. The global MPP powers of the generators are from 10% to 20% higher than nominal due to CE. The voltages of the global MPPs are from 5% to 7% higher than the nominal. Conversely, the perpendicular movement of the CE area does not cause irradiance differences within PV strings. Thus, there are only minor mismatch losses and the *P–U* curves are smooth (Lappalainen and Valkealahti, 2017). The global MPP powers are from 7% up to 40% larger than nominal, while the global MPP voltages are close to nominal.

D. Analysis during all the identified CE events

CE affects the global MPP voltages as illustrated in Fig. 10. Analysis of the operational voltage ranges of PV plants is useful to properly specify the voltage range of the inverter. Figure 11(a) presents the cumulative frequencies of the global MPP voltage for the studied PV generators during the identified CE events. The global MPP voltage was most of the time near the nominal value. The share of time when the global MPP voltage was higher than nominal increased with the increasing generator size. The global MPP voltage was within 2% of the nominal value 87%, 79%, and 69% of the time for the 6 × 16, 24 × 20, and 36 × 28 generators, respectively. The highest global MPP voltage was about 12% higher than the nominal value for all the studied PV generators.

The cumulative frequencies of the global MPP power are presented in Fig. 11(b) for the studied PV generators during the identified CE events. The global MPP power during the CE events typically increased with the smaller generator land area, as illustrated in Fig. 10. Thus, the share of time when the global MPP power was larger than nominal decreased with the larger generator size. However, the share was over 57% for all the studied generators. The share of time when the maximum power was more than 1.2 times the nominal MPP power was from 1.8% to 4.5% depending on the generator size. The maximum instantaneous power of all the studied PV generators was over 1.4 times the nominal MPP power.

Figure 12 presents the shares of time when the studied PV plants were operating in power limiting mode as a function of DC/AC ratio. The share of time when the PV plants were operating in power limiting mode increased with the decreasing plant size. With a 1.0 DC/AC

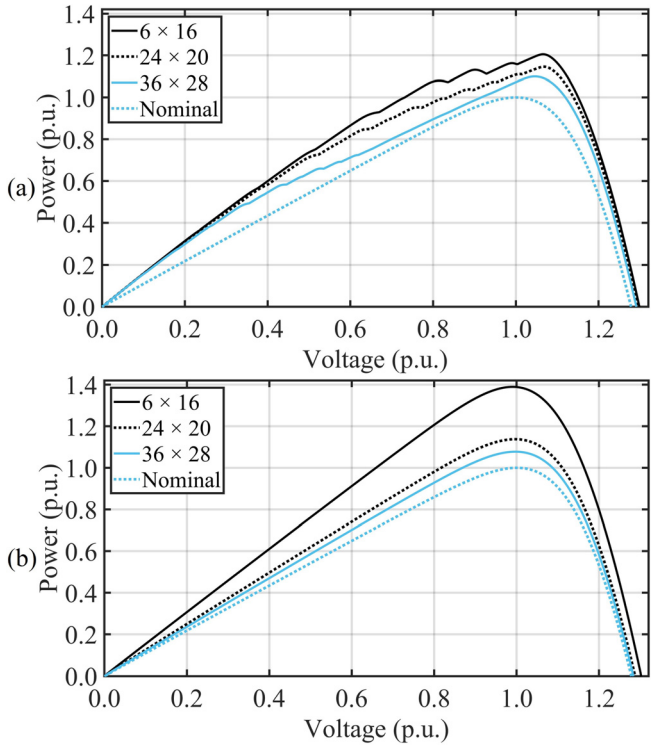

FIG. 10. Power–voltage curves of the studied PV generators in the examples of parallel (a) and perpendicular (b) CE area movement illustrated in Fig. 9. The values are presented with respect to the nominal STC values of the generators.

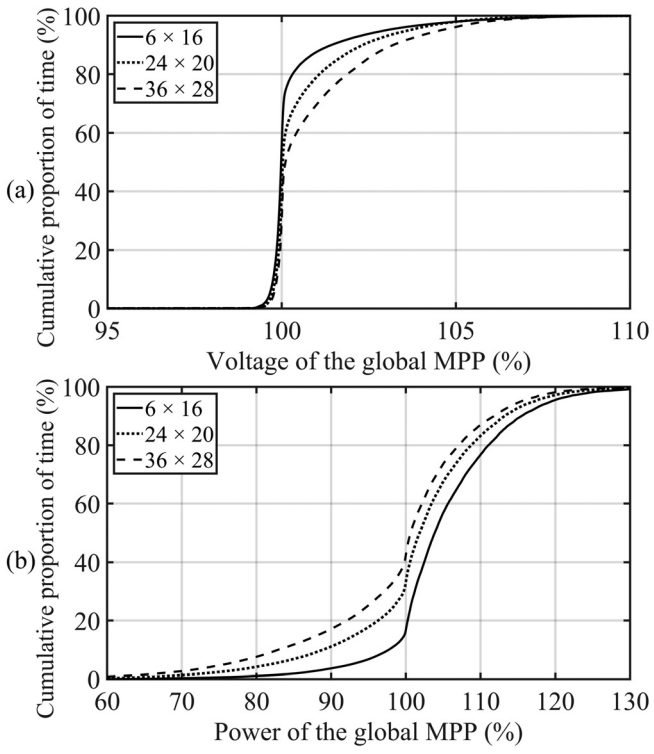

FIG. 11. Relative cumulative frequencies of the global MPP voltage (a) and power (b) for the studied PV generators during the identified CE events. Only CE events are considered in this graph, i.e., these statistics are not representative of overall PV operation.

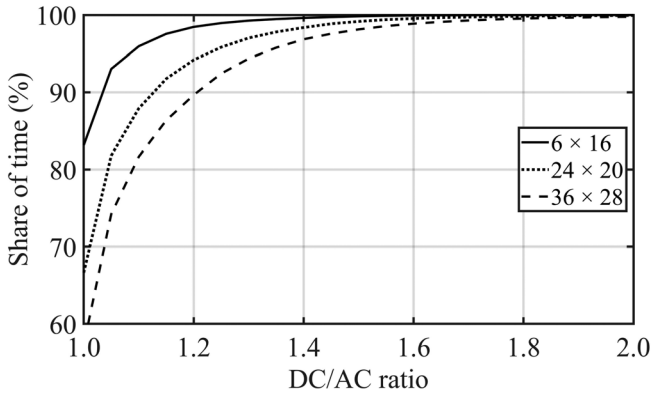

FIG. 12. Shares of time when the studied PV plants operated in power limiting mode as a function of DC/AC ratio. Only CE events are considered in this graph, i.e., these statistics are not representative of overall PV operation.

ratio, the PV plants were operating in power limiting mode from 57% to 83% and these shares increased rapidly with the increasing DC/AC ratio. The DC/AC ratios from which the PV plant was operating more than 99% of time in power limiting mode were 1.26, 1.47, and 1.63 for the 6 × 16, 24 × 20, and 36 × 28 plants, respectively.

Figure 13 presents the distributions of the operating voltage of the 36 × 28 PV plant for different DC/AC ratios. When the power of the generator was not limited, i.e., the generator operated all the time at the global MPP, the operating voltage was most of the time near the nominal MPP voltage. With a 1.0 DC/AC ratio, the peak of the voltage distribution is still near the nominal voltage, but the distribution spreads over a larger voltage range. With larger DC/AC ratios, the peak of the distribution moves toward higher voltages. Moreover, the distribution becomes narrower with the larger DC/AC ratio.

In Fig. 14, the highest and median operating voltages for studied PV plants are presented as a function of DC/AC ratio. There were only minor differences in the highest voltages between the studied PV plants. The highest voltages were from 17% to 25% higher than the nominal global MPP voltage. The median operating voltage increased

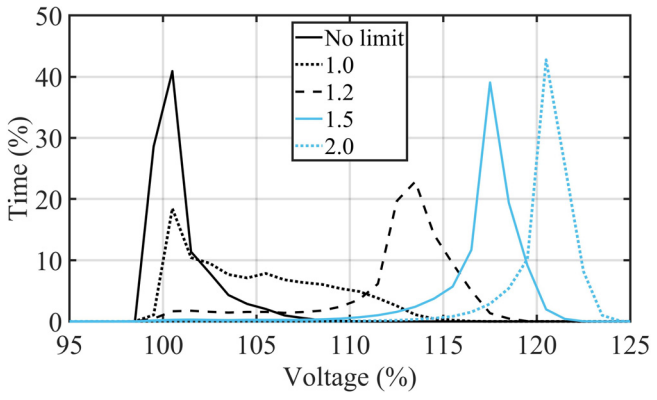

FIG. 13. Distributions of the operating voltage of the 36 × 28 plant for different DC/AC ratios. The voltage is with respect to the nominal MPP voltage of the plant. Only CE events are considered in this graph, i.e., these statistics are not representative of overall PV operation.

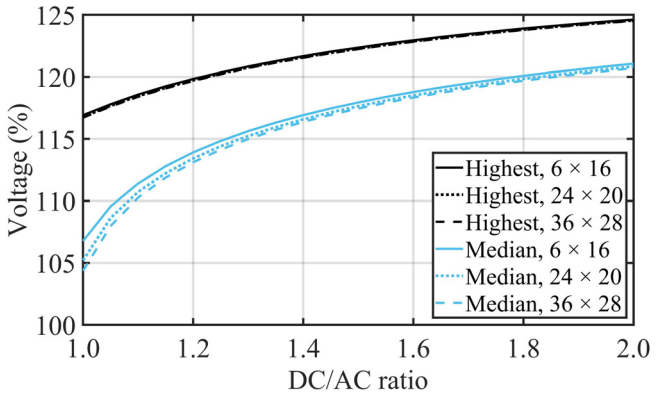

FIG. 14. Highest and median operating voltage as a function of DC/AC ratio. The voltage is with respect to the nominal MPP voltage of the plant. Only CE events are considered in this graph, i.e., these statistics are not representative of overall PV operation.

more with the increasing DC/AC ratio than the highest voltage. The operating voltage was higher for smaller plants. With DC/AC ratios larger than 1.85, the median operating voltage was over 20% higher than the nominal global MPP voltage. These results indicate that the increase in operating voltage due to CE is not a major problem for PV systems.

Operation in power limiting mode causes energy losses compared to the operation at the global MPP. These energy losses are presented in Fig. 15 for the studied PV plants as a function of DC/AC ratio. Relative energy losses due to power curtailment increased with the increasing DC/AC ratio since the larger the DC/AC ratio, the more the AC power is limited and the larger is the share of time spent in power limiting mode. While the differences between the studied plants were small, the relative energy losses increased with the decreasing plant size. With a DC/AC ratio of 1.0, the energy losses were around 5%, and with a DC/AC ratio of 2.0, about half of the available energy production was lost due to power curtailment. With small DC/AC ratios, the energy losses due to power curtailment are very small given the fact that only CE events were considered.

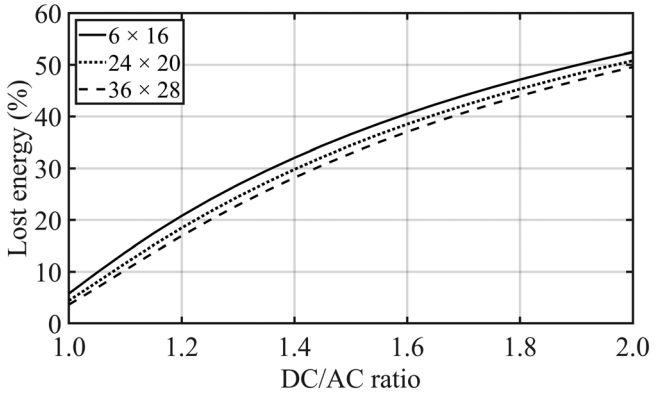

FIG. 15. Relative energy losses of the studied PV plants due to power curtailment as a function of DC/AC ratio. Only CE events are considered in this graph, i.e., these statistics are not representative of overall PV operation.

IV. DISCUSSION

The effects of CE on the operation of PV systems were shown to depend on the DC/AC ratio of the system. Specifically, the time spent in power limiting mode and the energy losses caused by power curtailment were found to increase with the increasing DC/AC ratio. With a small DC/AC ratio, the increase in operating voltages and the energy losses due to power curtailment are small, having only a minor impact on the overall operation of PV systems. However, relative energy losses due to curtailment increased with the increasing DC/AC ratio being around 50% for the DC/AC ratio of 2.0. Thus, oversizing of PV generators with respect to inverters is not recommended from the CE point of view. However, PV generators are typically oversized since oversizing of the PV generators brings many financial and operational benefits (Wang *et al.*, 2018). The optimal DC/AC ratio depends on many factors such as insolation conditions and inverter characteristics (Peippo and Lund, 1994). Peippo and Lund (1994) stated that the optimal DC/AC ratio region is quite flat and up to 20% changes from the optimal value typically lead to less than 2% losses. Zhu *et al.* (2011) recommended that the DC/AC ratio should be from 1.1 to 1.7. The results of this study show that if the intention is to avoid power curtailment caused by CE, the DC/AC ratio should be less than 1.0.

The relatively small increase in operating voltages due to CE, even with large DC/AC ratios (Fig. 14), indicates that CE does not cause increased risk of short-term equipment damage or disconnection for PV systems. However, the increasing operating voltage may cause further losses for PV systems since the increasing DC side voltage reduces the efficiency of some inverters. Moreover, the increasing operating voltage can affect the operating temperatures and lifetimes of certain components used in the inverters.

The negative impacts of CE on the operation of PV systems decreased with the increasing generator size, meaning that CE is less of a problem for utility-scale PV generators. CE events that have strongest impacts on the operation of PV systems are rare. In conclusion, the results of this study show that CE events do not cause major problems for the operation of PV systems. However, multiple assumptions and simplifications were applied in this study, which may affect the results. These issues have been discussed in the following paragraphs.

The CE event characteristics were based on the GHI measurements by a single sensor with a sampling frequency of 0.5 Hz. Measurements of multiple sensors spread over a large land area would be required to measure the actual irradiances and shapes of the CE areas accurately. It has been stated in Yordanov *et al.* (2013b) that a sampling frequency on the order of 10 Hz is needed to identify all CE events. However, a sampling frequency of 0.5 Hz is high enough to identify all CE events that affect the operation of PV generators. However, the uncertainty of CE event results increases with decreasing sampling frequency. Due to the low sampling frequency in our study, the durations of identified CE events are underestimated, short CE events might not be identified, and several CE events within a short time period might be aggregated into one event.

GHI measurements were used to study the effects of CE on the electrical operation of PV generators. The results would be more accurate if the actual plane of array irradiance measurements was used. Unfortunately, those were not available. The use of the actual plane of array irradiance measurements would probably lead to somewhat larger CE irradiances and longer CE events. However, the difference between GHI and the plane of array irradiance was relatively small due to the small tilt angle (20°).

In the simulations, three assumptions were made regarding the movement of the identified CE events over the PV generators (see Sec. III B). Although the assumptions are reasonable considering the small sizes of the studied PV generators, the uncertainty of the results increases with larger land areas. Specifically, the assumption of irradiance uniformity in the cross-stream direction might not hold for larger land areas. Moreover, the operating temperature of the PV generators was assumed to be constant. The operating temperature of the PV cells of a PV generator in California, especially during CE events, can be much higher than the STC temperature. The OC voltage and MPP power of a PV cell decrease, and the SC current increases slightly with increasing temperature. Thus, the assumption of constant temperature affects mainly the results of the global MPP and operating voltages. However, the use of STC temperature, which is almost always lower than real operating temperatures, leads to an overestimation of the operating voltages. Thus, real operating voltages are expected to be smaller than that reported in this study.

The electrical simulation model for the PV modules naturally contains assumptions and simplifications. First, a PV submodule was used as a basic unit in the simulations. However, only negligible irradiance differences between the PV cells of a submodule existed during the studied CE events. Thus, the results of this study would change only marginally if the simulation were conducted at a PV cell level. Second, the PV submodules were modeled by the widely used one-diode model of a PV cell, which is a simplification of the more accurate two-diode model. However, the one-diode model provides a good trade-off between accuracy and complexity and is accurate enough for the analysis that was presented in this article. Moreover, the results could slightly change if different PV modules were used as a reference for the simulation model. However, the basic behavior would not change since the electrical characteristics of crystalline silicon PV modules are essentially identical. Crystalline silicon was selected as it is by far the most important PV technology.

V. CONCLUSIONS

In this article, CE event characteristics and the effects of CE on the electrical operation of PV generators were studied. This study was based on GHI and cloud edge velocity measurements on 62 days. The number, duration, and length of CE events exceeding various irradiance limits from 1000 W/m^2 over the land areas of various PV generators were studied. The average irradiance over the land areas was calculated by averaging the measured GHI over a time interval defined by the ratio of the PV generator dimension and the measured cloud shadow speed. Moreover, the operation of three PV generators, ranging from 20 to 200 kW, was simulated during all CE events. The effects of inverter sizing on the operation of the PV generators were studied by varying the DC/AC ratio from 1.0 to 2.0.

In total, 2401 CE events exceeding 1000 W/m^2 were identified in the measured GHI. The average irradiance of the 0.05 and 4 MW generators exceeded the STC irradiance over 1500 and 400 times, respectively. The highest measured peak irradiance was 1466 W/m^2, and the highest average irradiances for the studied PV generators up to 1 MW were also over 1400 W/m^2. The maximum durations of CE events exceeding 1300 W/m^2 were around one minute. The largest lengths for CE events exceeding 1000 W/m^2 were multiple kilometers.

A square-shaped PV generator of up to 16 MW can occasionally be totally covered by a CE area with a minimum irradiance of over 1200 W/m^2. These results mean that even large utility-scale PV power plants can be affected by CE events.

The simulation results showed that CE affects the operation of the PV plants, but the effects are mainly small. Although the highest global MPP voltage and power were about 12% and 40% higher than the nominal STC values, the global MPP voltage was most of the time near the nominal value. The negative impacts of CE on the operation of PV systems were found to increase with the increasing DC/AC ratio. With a DC/AC ratio of 1.0, all the PV plants were operating in power limiting mode over half of the time of the CE events and these shares increased rapidly with the increasing DC/AC ratio. The highest operating voltages were from 17% to 25% higher than the nominal global MPP voltage. The operating voltage increased with the increasing DC/AC ratio and decreasing plant size. With DC/AC ratios larger than 1.85, the median operating voltage was over 20% higher than the nominal global MPP voltage. The energy losses due to power curtailment were from 5% to 50% of the available energy production during the CE events increasing with the increasing DC/AC ratio. To avoid power curtailment caused by CE, DC/AC ratios should be less than 1.0. In conclusion, the results of this study show that CE does not cause major problems for the operation of PV systems.

ACKNOWLEDGMENTS

The Alfred Kordelin Foundation funded the research visit of K. Lappalainen to UCSD during which the study presented in this article was carried out.

APPENDIX: CALCULATION OF CLOUD MOTION VECTORS

The CSS detects the component of cloud shadow velocity normal to the shadow edge, i.e., cloud shadow edge velocity, $\boldsymbol{v}_e$ (speed v_e and movement direction α_e), which underestimates the actual shadow velocity $\boldsymbol{v}$ (speed v and movement direction α). A weighted non-linear regression of v and α to the N_{CMV} CMVs collected in a time period of 30 min was used to calculate $\boldsymbol{v}$ from $\boldsymbol{v}_e$ as

$$w_i v_e^i = v\cos\left(\alpha_e^i - \alpha\right), \tag{A1}$$

where w_i is a weighting factor calculated as

$$w_i = |t_f - t_o| - |t_i - t_o| + 1, \tag{A2}$$

where t_f is the timestamp furthest from the present time t_o in the time period and t_i the timestamp of the ith CMV. If the CMVs collected in the time period show variation of α_e smaller than 20°, the shadow movement direction is almost perpendicular to the shadow edge and the non-linear regression is not needed. In these cases, and if N_{CMV} is too small for reliable regression (less than 9), the CMVs are decomposed into north–south and east–west directions, and the median value of each is used to recompose the resulting CMV.

DATA AVAILABILITY

The data that support the findings of this study are available from the corresponding author upon reasonable request.

REFERENCES

Badescu, V., "Verification of some very simple clear and cloudy sky models to evaluate global solar irradiance," Sol. Energy **61**, 251–264 (1997).
Callegari, J. M. S., Cupertino, A. F., Ferreira, V. N., Brito, E. M. S., Mendes, V. F., and Pereira, H. A., "Adaptive DC-link voltage control strategy to increase PV inverter lifetime," Microelectron. Reliab. **100–101**, 113439 (2019).
do Nascimento, L. R., de Souza Viana, T., Campos, R. A., and Rüther, R., "Extreme solar overirradiance events: Occurrence and impacts on utility-scale photovoltaic power plants in Brazil," Sol. Energy **186**, 370–381 (2019).
Espinosa-Gavira, M. J., Agüera-Pérez, A., de la Rosa, J. J. G., Palomares-Salas, J. C., and Sierra-Fernández, J. M., "An on-line low-cost irradiance monitoring network with sub-second sampling adapted to small-scale PV systems," Sensors **18**, 3405 (2018).
Gueymard, C. A., "Cloud and albedo enhancement impacts on solar irradiance using high-frequency measurements from thermopile and photodiode radiometers. Part 1: Impacts on global horizontal irradiance," Sol. Energy **153**, 755–765 (2017a).
Gueymard, C. A., "Cloud and albedo enhancement impacts on solar irradiance using high-frequency measurements from thermopile and photodiode radiometers. Part 2: Performance of separation and transposition models for global tilted irradiance," Sol. Energy **153**, 766–779 (2017b).
Hasegawa, K., Tsuzaki, K., and Nishizawa, S., "DC-bias-voltage dependence of degradation of aluminum electrolytic capacitors," Microelectron. Reliab. **83**, 115–118 (2018).
Imenes, A. G., Yordanov, G. H., Midtgård, O.-M., and Saetre, T. O., "Development of a test station for accurate in situ I-V curve measurements of photovoltaic modules in Southern Norway," in Proceedings of the 37th IEEE Photovoltaic Specialists Conference (2011), pp. 3153–3158.
Järvelä, M., Lappalainen, K., and Valkealahti, S., "Cloud enhancement phenomenon and its effect on PV generators," in Proceedings of 35th European Photovoltaic Solar Energy Conference (2018), pp. 1964–1968.
Järvelä, M., Lappalainen, K., and Valkealahti, S., "Characteristics of the cloud enhancement phenomenon and PV power plants," Sol. Energy **196**, 137–145 (2020).
Lappalainen, K. and Valkealahti, S., "Recognition and modelling of irradiance transitions caused by moving clouds," Sol. Energy **112**, 55–67 (2015).
Lappalainen, K. and Valkealahti, S., "Analysis of shading periods caused by moving clouds," Sol. Energy **135**, 188–196 (2016).
Lappalainen, K. and Valkealahti, S., "Effects of PV array layout, electrical configuration and geographic orientation on mismatch losses caused by moving clouds," Sol. Energy **144**, 548–555 (2017).
Luoma, J., Kleissl, J., and Murray, K., "Optimal inverter sizing considering cloud enhancement," Sol. Energy **86**, 421–429 (2012).
Mäki, A., Valkealahti, S., and Leppäaho, J., "Operation of series-connected silicon-based photovoltaic modules under partial shading conditions," Prog. Photovoltaics: Res. Appl. **20**, 298–309 (2012).
Ong, S., Campbell, C., Denholm, P., Margolis, R., and Heath, G., "Land-use requirements for solar power plants in the United States," Report No. NREL/TP-6A20-56290 (National Renewable Energy Laboratory, Golden, CO, USA, 2013).
Pecenak, Z. K., Mejia, F. A., Kurtz, B., Evan, A., and Kleissl, J., "Simulating irradiance enhancement dependence on cloud optical depth and solar zenith angle," Sol. Energy **136**, 675–681 (2016).
Peippo, K. and Lund, P. D., "Optimal sizing of solar array and inverter in grid-connected photovoltaic systems," Sol. Energy Mater. Sol. Cells **32**, 95–114 (1994).
Rampinelli, G. A., Krenzinger, A., and Chenlo Romero, F., "Mathematical models for efficiency of inverters used in grid connected photovoltaic systems," Renewable Sustainable Energy Rev. **34**, 578–587 (2014).
Tapakis, R. and Charalambides, A. G., "Enhanced values of global irradiance due to the presence of clouds in eastern Mediterranean," Renewable Energy **62**, 459–467 (2014).
Tomson, T., "Transient processes of solar radiation," Theor. Appl. Climatol. **112**, 403–408 (2013).
Wang, G., Kurtz, B., and Kleissl, J., "Cloud base height from sky imager and cloud speed sensor," Sol. Energy **131**, 208–221 (2016).

Wang, H. X., Munoz-García, M. A., Moreda, G. P., and Alonso-García, M. C., "Optimum inverter sizing of grid-connected photovoltaic systems based on energetic and economic considerations," Renewable Energy **118**, 709–717 (2018).
Weigl, T., Nagl, L., Weizenbeck, J., Zehner, M., Augel, M., Öchsner, P., Giesler, B., Becker, G., Mayer, O., Betts, T. R., and Gottschalg, R., "Modelling and validation of spatial irradiance characteristics for localised irradiance fluctuations and enhancements," in Proceedings of 27th European Photovoltaic Solar Energy Conference (2012), pp. 3801–3804.
Yordanov, G. H., Midtgård, O.-M., Saetre, T. O., Nielsen, H. K., and Norum, L. E., "Overirradiance (cloud enhancement) events at high latitudes," IEEE J. Photovoltaics **3**, 271–277 (2013a).
Yordanov, G. H., Saetre, T. O., and Midtgård, O.-M., "100-millisecond resolution for accurate overirradiance measurements," IEEE J. Photovoltaics **3**, 1354–1360 (2013b).
Yordanov, G. H., Saetre, T. O., and Midtgård, O.-M., "Extreme overirradiance events in Norway: 1.6 suns measured close to 60°N," Sol. Energy **115**, 68–73 (2015).
Zehner, M., Weigl, T., Hartmann, M., Thaler, S., Schrank, O., Czakalla, M., Mayer, B., Betts, T. R., Gottschalg, R., Behrens, K., König-Langlo, G., Giesler, B., Becker, G., and Mayer, O., "Energy loss due to irradiance enhancement," in Proceedings of 26th European Photovoltaic Solar Energy Conference (2011), pp. 3935–3938.
Zhang, J., Watanabe, K., Yoshino, J., Kobayashi, T., Hishikawa, Y., and Doi, T., "Physical process and statistical properties of solar irradiance enhancement observed under clouds," Jpn. J. Appl. Phys., Part 1 **57**, 08RG11 (2018).
Zhu, J., Bründlinger, R., Mühlberger, T., Betts, T. R., and Gottschalg, R., "Optimised inverter sizing for photovoltaic systems in high-latitude maritime climates," IET Renewable Power Gener. **5**, 58–66 (2011).